

Production of biofunctionalized MoS₂ flakes with rationally modified lysozyme: a biocompatible 2D hybrid material

This content has been downloaded from IOPscience. Please scroll down to see the full text.

2017 2D Mater. 4 035007

(<http://iopscience.iop.org/2053-1583/4/3/035007>)

View [the table of contents for this issue](#), or go to the [journal homepage](#) for more

Download details:

IP Address: 143.225.69.60

This content was downloaded on 10/07/2017 at 11:59

Please note that [terms and conditions apply](#).

You may also be interested in:

[Luminescent transition metal dichalcogenide nanosheets through one-step liquid phase exfoliation](#)

M Mar Bernal, Lidia Álvarez, Emerson Giovanelli et al.

[Thermoelectric performance of restacked MoS₂ nanosheets thin-film](#)

Tongzhou Wang, Congcong Liu, Jingkun Xu et al.

[Self-assembled peptide nanostructures for functional materials](#)

Melis Sardan Ekiz, Goksu Cinar, Mohammad Aref Khalily et al.

[Industrial grade 2D molybdenum disulphide \(MoS₂\): an in vitro exploration of the impact on cellular uptake, cytotoxicity, and inflammation](#)

Caroline Moore, Dania Movia, Ronan J Smith et al.

[Effect of post-exfoliation treatments on mechanically exfoliated MoS₂](#)

P Budania, P T Baine, J H Montgomery et al.

[Engineering chemically exfoliated dispersions of two-dimensional graphite and molybdenum disulphide for ink-jet printing](#)

Monica Michel, Jay A Desai, Chandan Biswas et al.

[Chemically exfoliating large sheets of phosphorene via choline chloride urea viscosity-tuning](#)

A Ng, T E Sutto, B R Matis et al.

[Small interfering RNA delivery through positively charged polymer nanoparticles](#)

Luca Dragoni, Raffaele Ferrari, Monica Lupi et al.

[Soft exfoliation of 2D SnO with size-dependent optical properties](#)

Mandeep Singh, Enrico Della Gaspera, Taimur Ahmed et al.

2D Materials



PAPER

Production of biofunctionalized MoS₂ flakes with rationally modified lysozyme: a biocompatible 2D hybrid material

RECEIVED
14 March 2017

REVISED
30 May 2017

ACCEPTED FOR PUBLICATION
14 June 2017

PUBLISHED
6 July 2017

Marialuisa Siepi^{1,2}, Eden Morales-Narváez¹, Neus Domingo¹, Daria Maria Monti³, Eugenio Notomista² and Arben Merkoçi¹

¹ Nanobioelectronics and Biosensor Group, Catalan Institute of Nanoscience and Nanotechnology (ICN2), CSIC, The Barcelona Institute of Science and Technology, Campus UAB, Bellaterra, 08193 Barcelona, Spain

² Department of Biology University of Naples Federico II, Via Cintia, 80126 Naples, Italy

³ Department of Chemical Sciences University of Naples Federico II, Via Cintia, 80126 Naples, Italy

⁴ ICREA, Pg. Lluís Companys 23, 08010 Barcelona, Spain

E-mail: arben.merkoci@icn2.cat

Keywords: 2D materials, biocompatibility, biofunctionalized material, MoS₂

Supplementary material for this article is available [online](#)

Abstract

Bioapplications of 2D materials embrace demanding features in terms of environmental impact, toxicity and biocompatibility. Here we report on the use of a rationally modified lysozyme to assist the exfoliation of MoS₂ bulk crystals suspended in water through ultrasonic exfoliation. The design of the proposed lysozyme derivative provides this exfoliated 2D-material with both, hydrophobic groups that interact with the surface of MoS₂ and hydrophilic groups exposed to the aqueous medium, which hinders its re-aggregation. This approach, clarified also by molecular docking studies, leads to a stable material (ζ -potential, 27 ± 1 mV) with a yield of up to $430 \mu\text{g ml}^{-1}$. The bio-hybrid material was characterized in terms of number of layers and optical properties according to different slots separated by diverse centrifugal forces. Furthermore the obtained material was proved to be biocompatible using human normal keratinocytes and human cancer epithelial cells, whereas the method was demonstrated to be applicable to produce other 2D materials such as graphene. This approach is appealing for the advantageous production of high quality MoS₂ flakes and their application in biomedicine and biosensing. Moreover, this method can be applied to different starting materials, making the denatured lysozyme a promising bio-tool for surface functionalization of 2D materials.

Introduction

Two dimensional (2D) materials possess outstanding properties that are opening the path to a wide range of unprecedented scientific and technological applications [1]. Among the emerging 2D materials, molybdenum disulphide (MoS₂) is particularly interesting due to its potential applications in catalysis [2], opto/electronics [3, 4] and biomedicine [5, 6]. As a transitional metal dichalcogenide, MoS₂ is a semiconductor with an indirect bandgap of about 1.2 eV in the bulk form [7–9]. Though, decreasing the thickness of this material, from the bulk to the monolayer, the band gap of MoS₂ increases to 1.9 eV [10]. Moreover, it changes from indirect to direct band [2]. In addition, recent works report that MoS₂ in the form of a few-layer or monolayer crystal is photoluminescent, which is attributed to the direct gap in the electronic

structure of MoS₂ [11–13]. Consequently, this novel material is appealing for innovative photovoltaic and photocatalytic applications [14–16] and the generation of MoS₂ monolayers is a critical step for the development of novel devices based on this 2D material [17].

Single-layer MoS₂ can be viewed as an ‘S–Mo–S’ sandwich structure, in which a plane of molybdenum atoms is layered between two planes of sulphur atoms. Each Mo is coordinated to six S atoms according to a trigonal prismatic geometry. As the stacked S–Mo–S layers are bound by weak van der Waals interactions [18, 19], it is possible to generate individual MoS₂ nano/micro sheets by exfoliation of bulk MoS₂ crystals [20, 21].

Several approaches have been developed for the production of MoS₂. The simplest strategy is a micro-mechanical cleavage using the scotch-tape method [4, 22, 23]. This method leads to the production of high

quality material but is not suitable for the large-scale production of MoS₂ due to the low yield, and to the fact that the size and thickness of the resultant MoS₂ micro/nanosheets are difficult to control. Chemical vapour deposition allows for the production of high quality MoS₂ sheets with excellent yield, but the complex experimental requirements limit the wide applicability of the method [20, 24, 25]. Compared to the aforementioned methods, liquid-phase exfoliation provides large quantity of high quality flakes at low costs [26]. Typically, liquid-phase exfoliation involves the use of ultrasonication in organic solvents [27–29], such as N-methylpyrrolidone and dimethylformamide, or in water in the presence of suited surfactants [30, 31]. After their preparation, the micro/nanosheets can be easily sorted and separated [32], resulting in a desirable size and thickness, moreover, by changing the solvent or the surfactant it is possible to obtain materials with different properties and applications.

Biomedical applications of MoS₂ involve major concerns such as environmental impact, toxicity and biocompatibility [6, 33]. The use of biomolecules, such as proteins, during the exfoliation leads to several advantages including a low environmental impact, biocompatibility of the resulting material, and easier functionalization of the flakes avoiding covalent modifications that could change the properties of the material. In fact, bioconjugation of MoS₂ sheets is crucial for different applications in the biotechnological and biomedical fields (i.e. drug delivery, tissue engineering, biosensors, scaffolds, etc) [21, 34]. During the last years, several approaches have been developed for the liquid-phase exfoliation of MoS₂ using biomolecules, such as polysaccharides [35–37], DNA/RNA nucleotides [34, 37], and proteins [38–40].

Recently, Guan *et al* reported the production of water soluble MoS₂ using bovine serum albumin (BSA) [39]. MoS₂ powder was sonicated during 48 h with BSA obtaining exfoliated/soluble material whose maximum concentration was 1.36 mg ml⁻¹, with a production rate of 0.38 μg ml⁻¹ h⁻¹.

More recently, Forsberg *et al* reported a different approach to obtain MoS₂ in water, by combining mechanical and liquid exfoliation, and obtaining 0.14 mg ml⁻¹ of MoS₂ after 1 h sonication [41], a value lower than that obtained by Guan [39]. Ayan-Varela *et al* reported the use of nucleotides to solubilize MoS₂, obtaining a dispersion with a yield which was inversely related to nucleotide concentration, reaching a maximum of 5–10 mg ml⁻¹ (production rate of 1–2 mg ml⁻¹ h⁻¹). However, the thickness of the flakes was inversely related to nucleotide concentration, with smaller and thinner flakes present at higher nucleotide concentration [34]. Thus, even if in the last few years important advances have been achieved in the field of the MoS₂ exfoliation with biomolecules, obtaining a biocompatible material still is not completely investigated. Furthermore, the development of fast and universal approach for the large-scale production of MoS₂, also applied to differ-

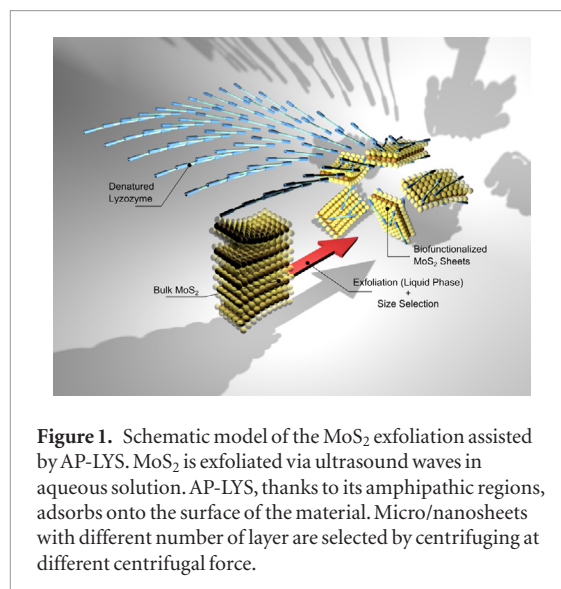


Figure 1. Schematic model of the MoS₂ exfoliation assisted by AP-LYS. MoS₂ is exfoliated via ultrasound waves in aqueous solution. AP-LYS, thanks to its amphiphilic regions, adsorbs onto the surface of the material. Micro/nanosheets with different number of layer are selected by centrifuging at different centrifugal force.

ent 2D materials, aiming to obtain materials endowed with unique properties, is still a challenge.

We believe that MoS₂ exfoliation in the liquid phase can be benefited by using a rationally modified protein endowed with specific amphiphilic properties that is with hydrophobic groups able to interact with the surface of MoS₂ and hydrophilic groups exposed to the aqueous medium which should stabilize the delaminated material and prevent its re-aggregation. Herein, we designed a denatured, stable and fully soluble lysozyme derivative bearing amino-propyl moieties bound to the eight cysteine residues (aminopropyl-lysozyme, AP-LYS) [42], which is able to promote the formation of highly stable protein-decorated MoS₂ flakes. We report the production of biofunctionalized MoS₂ using liquid-phase exfoliation via ultrasound waves in the presence of AP-LYS. As depicted in figure 1, the bulk form of the material was ultrasonicated in aqueous solution. Subsequently, AP-LYS, thanks to its amphiphilic region, is adsorbed onto the exfoliated MoS₂, stabilizing and functionalizing the exfoliated material. Centrifugations at different centrifugal forces were performed to control and select flakes with different size, obtaining a highly stable material. Docking studies were also performed to propose a theoretical model of the interaction between the rationally modified protein and the exfoliated MoS₂. The production optimization, biofunctionalization, number of layers, stability, optical properties, yield and potential biocompatibility were systematically studied and the applicability of the method to produce other 2D materials such as graphene was also confirmed.

This approach can be applied for a large scale production of MoS₂ increasing its biocompatibility and dispersibility for various applications. This method allows the utilization of low-cost precursors, such as a powder, avoiding the addition of organic solvent.

The bio-hybrid material is endowed of unique properties and applicability in biotechnological and biomedical field.

Methods

Docking of lysozyme fragment 1–18

The interaction of fragment 1–18 of lysozyme with the surface of a MoS₂ monolayer was modelled by using a Monte Carlo energy minimization strategy which has already proved useful for the modelling of several complexes between biological macromolecules and ligands of different nature and size [43–47]. All calculations were performed using the ZMM-MVM molecular modelling package (ZMM Software Inc. (www.zmmsoft.com)). ZMM software allows conformational searches using generalized coordinates (e.g. torsion and bond angles) instead of conventional Cartesian coordinates [48], thus making the conformational search faster and much more efficient than usually obtained with other methods. Atom–atom interactions were evaluated using the Amber force fields [49] with a cutoff distance of 8 Å. Conformational energy calculations included van der Waals, electrostatic, H bond, and torsion components. Electrostatic interactions were calculated using an environment- and distance-dependent dielectric permittivity according to a method implemented in the ZMM software. Energy calculations also included a hydration component calculated as previously described [50, 51]. The model included lysozyme fragment 1–18 and a MoS₂ monolayer.

The monolayer contained 1020 MoS₂ units arranged to form a square with a side of about 91 Å. Partial charges assigned to Mo and S atoms were +0.22 and –0.11 [52]. The MoS₂ monolayer was frozen throughout the simulation process.

The sequence of the modelled lysozyme fragment was NH₂-KVFGRCELAAAMKRHGLD-CONH₂. We choose to model an amidated C-terminus in order not to insert a negative charge not present in the protein. Cysteine at position 6 was modelled as an aminopropylcysteine. Histidine at position 17 was modelled in the protonated form as all the exfoliation experiments were conducted at pH 5. Initial structures of the fragment were prepared using PyMOL (DeLano Scientific LLC, www.pymol.org/) and DeepView—Swiss-PdbViewer [53]. Two initial structures were modelled, a completely helical and a completely extended structure. Each structure was used to generate four starting manually prepared complexes: fragment 1–18 was placed parallel to the surface, along one of the diagonals of the MoS₂ monolayer, hence the peptide structure was rotated by steps of 90°. Each of the eight models was used as starting point for a Monte Carlo trajectory. Trajectories were stopped when no energy decrease was observed for 1000 minimization cycles.

Exfoliation process

Molybdenum disulphide powder (Aldrich, 234842), was shaken using a TS-100 Thermo-Shaker (Biosan, Riga, Latvia) at 650 rpm over night at 4 °C in batches of 5 ml of 10 mM Sodium Acetate pH 5 with 0.2–1

mg ml^{–1} AP-LYS [42], and then sonicated with a medium power tip sonicator (Q125 Sonicor, QSonica, 125 W, 20 kHz, inbuilt power meter power output, 19 W) in an ice bath. The dispersion was centrifuged at different centrifugal force using a Sigma 1–15 Fisher Bioblock scientific centrifuge. The UV–Vis spectra of the supernatants were acquired using UV–vis spectrophotometer Cary 4000 Scan using a quartz cell 1 cm optics. Concentration of dispersion was estimated by UV–vis spectroscopy, using the linear relationship of the concentration and absorption intensity at 666 nm previously established by Guan *et al* [39].

Graphite powder (Aldrich, 332461) (2 mg ml^{–1}) was exfoliated as previously described in the presence of AP-LYS (0.2 mg ml^{–1}). After consecutive centrifugations at 40, 2500 and 4500 g, the concentration of dispersions were determined using the absorption coefficient value at 660 nm (1390 g l cm^{–1}), as previously reported [54].

Characterization

Photoluminescence has been performed using a Hitachi F-2500 spectrometer. The sample was excited at 342 nm. The emission spectra were recorded in the range 383–600 nm.

Scanning electron microscopy (SEM) were performed by dropping 3 μl of solution on silicon chip. Images were recorded using FEI Quanta 650 FEG ESEM, 2 kV microscope.

AFM measurements were performed on silicon chip using a Nanoscope V Multimode8 AFM (Bruker, Germany) and Si cantilevers (SNL model, k : 0.3 N m^{–1}, Bruker). The scanning probe microscopy was carried out at a scan rate of 1 Hz and 512 × 512 pixel. The silicon chip was dipped in the solution and dried by evaporation at room temperature under a ventilated fume hood. Electrokinetic analysis and ζ-potential were carried out in folded capillary cells using a Malvern Zetasizer Nano-ZS system equipped with a 633 nm He–Ne laser. All measurements were conducted at 25 °C. For the Raman spectroscopy, samples were dropped on corning microscope glass slides (Aldrich, CLS294775 × 25), laser was focused on samples and multiple spectra were accumulated. The spectra were recorded with Horiba JobinYvonLabRAM HR 800, 800 mm focal length, 100× objective, excitation wavelength 532 nm.

Biocompatibility

2000 HeLa cells and 5000 HaCaT cells were seeded in 96 well-plates as monolayer. After 24 h, cells were incubated in the presence of increasing concentration of AP-LYS/MoS₂ sample (5–10–20–50–100 μg ml^{–1}) for 24–48 h, in complete medium at 37 °C in a humidified atmosphere containing 5% CO₂. At the end of incubation, AlamarBlue® reagent (Invitrogen) was added in each well and incubated for 3 h at 37 °C. The fluorescence intensity was measured at an emission wavelength of 585 nm and an excitation wavelength of 570 nm using a plate reader (Synergy HTX Multi-

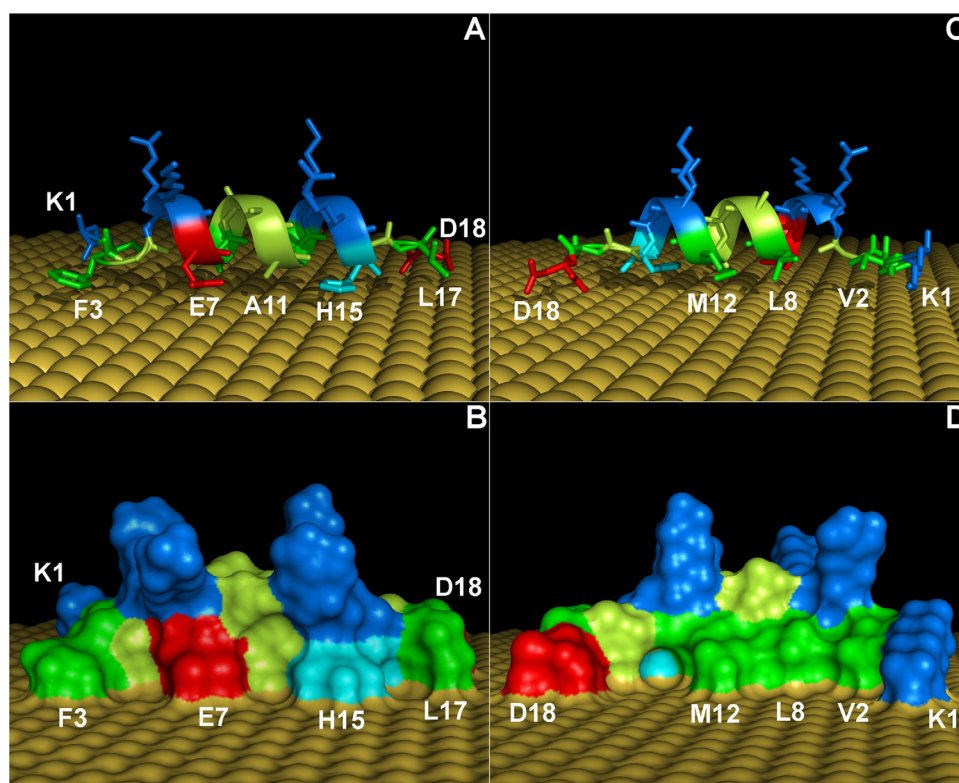


Figure 2. Docking of fragment 1–18 of hen egg lysozyme onto the surface of a MoS₂ monolayer. Residues are colored according to their properties: green, hydrophobic; light green, borderline residues (alanine, glycine); blue, positively charged; red, negatively charged; cyan, histidine. In panels (A) and (C) the protein fragment is shown as cartoon and sticks to highlight the secondary structure of the peptide and the side chains contacting the sulfur atoms of the surface (shown as dark yellow spheres). In panel (C) the structure is rotated by 180° around an axis perpendicular to the surface as compared to panel (A). Panels (B) and (D) show the solvent accessible surface of the complex for the orientations shown in panels (A) and (C), respectively. Labels are shown only for the residues making significant interaction with the surface (the corresponding binding energy values and the number of surface sulfur atoms involved in the interaction are shown in table S1).

Mode Reader-BIOTEK). Cell survival was expressed as the percentage of viable cells in the presence of the AP-LYS/MoS₂ sample compared to controls. Two groups of cells were used as control, i.e. untreated cells and cells supplemented with identical volumes of buffer. Each sample was tested in three independent analyses, each carried out in triplicate. Quantitative parameters were expressed as the mean value \pm SD. Significance was determined by Student's *t*-test at a significance level of 0.05.

Result and discussion

Molecular docking analysis

As we have discussed previously, the ability of AP-LYS to promote the solubilisation of hydrophobic materials is likely related to the fact that the denaturation process significantly increases the molecular surface and the flexibility of lysozyme, and exposes to the solvent hydrophobic residues usually buried inside the hydrophobic core of the native protein [42]. However, even if AP-LYS is essentially unfolded in water, it is prone to regain a significant content of helical structure in the presence of trifluoroethanol [55–60], an organic solvent widely used to mimic the interaction of protein and peptide with detergent micelles and biological

membranes. Very interestingly previous studies suggest that this increased content of helical structure is likely due to the refolding of the amphipathic α -helices located at the N- and C-terminus of the native lysozyme [61]. On the basis of these observations it can be hypothesized that the interaction of AP-LYS with 2D materials like MoS₂ and graphene is due to an adsorption process of amphipathic secondary elements of the denatured protein onto the hydrophobic surface of these materials. The high positive charge of the hydrophilic sides would then stabilize the exfoliated material in water. In order to verify this hypothesis we modeled the interaction of residues 1–18 of lysozyme, which include the first amphipathic α -helix (residues 4–15), with a MoS₂ monolayer. The search for the lowest energy complex was performed by a Monte Carlo-based strategy starting from two limit structures— α -helix or extended—each placed in four different orientations above the MoS₂ sheet (see figure 2). In the lowest energy complex the lysozyme fragment adopts a structure which is intriguingly similar to that observed in the native protein. In fact, residues 5–15 form an amphipathic α -helix with the hydrophobic residues Leu-8, Ala-11 and Met-12 and two adjacent hydrophilic residues (Glu-7 and His-15) closely packed onto the surface. Residues 1–4, which in the native protein are

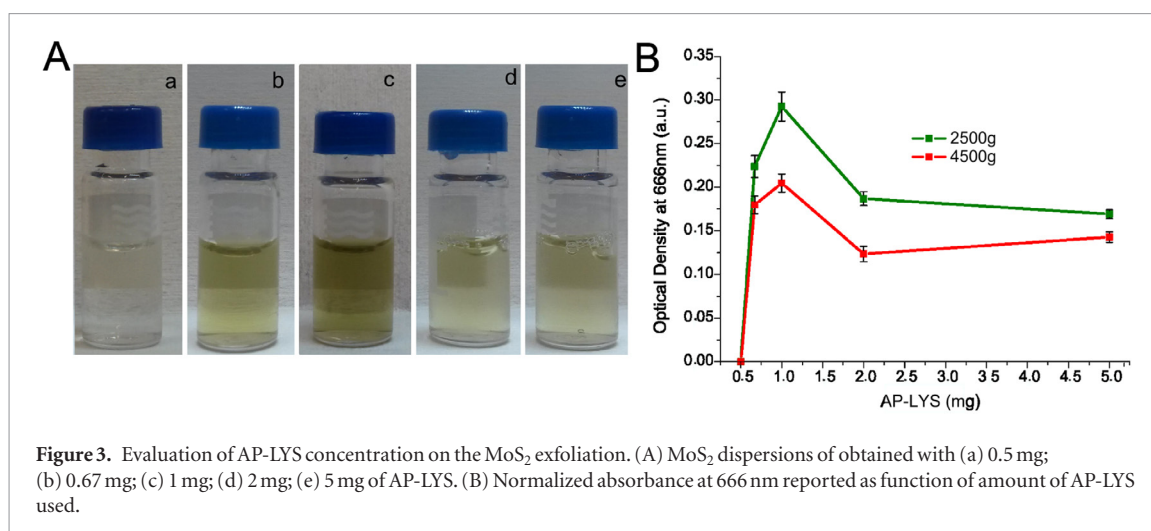
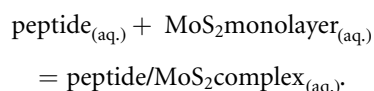


Figure 3. Evaluation of AP-LYS concentration on the MoS₂ exfoliation. (A) MoS₂ dispersions of obtained with (a) 0.5 mg; (b) 0.67 mg; (c) 1 mg; (d) 2 mg; (e) 5 mg of AP-LYS. (B) Normalized absorbance at 666 nm reported as function of amount of AP-LYS used.

folded to pack the hydrophobic residues Val-2 and Phe-3 against the hydrophobic core in the complex, form a turn allowing these two residues to contact the surface of the MoS₂ monolayer. Similarly residues 16–18 adopt a non-helical conformation allowing the binding of residues Leu-17 and Asp-18 to the surface. Table S1 shows the residues whose contribution to the binding energy is higher than 0.1 kcal mol⁻¹. Not surprisingly the highest contributions are from Phe-3 and His-15 due to a stacking interaction between the rings in the side chains of these residues and the surface. These two residues also show the highest average contribution per sulphur atom on the surface. This result is due to the high polarizability of the pi systems in the side chains of phenylalanine and histidine which determines stronger van der Waals interactions. Interestingly three hydrophilic residues, Lys-1, Glu-7, and Asp-18, contribute significantly to the binding energy. In the case of Glu-7, the planar moiety –CH₂–COO⁻ lays parallel to the MoS₂ surface. Similarly in the case of Lys-1, the terminal moiety –CH₂–NH₃⁺ lays close to the surface. In the case of Asp-18 both the main-chain and the side-chain make van der Waals interaction with the surface.

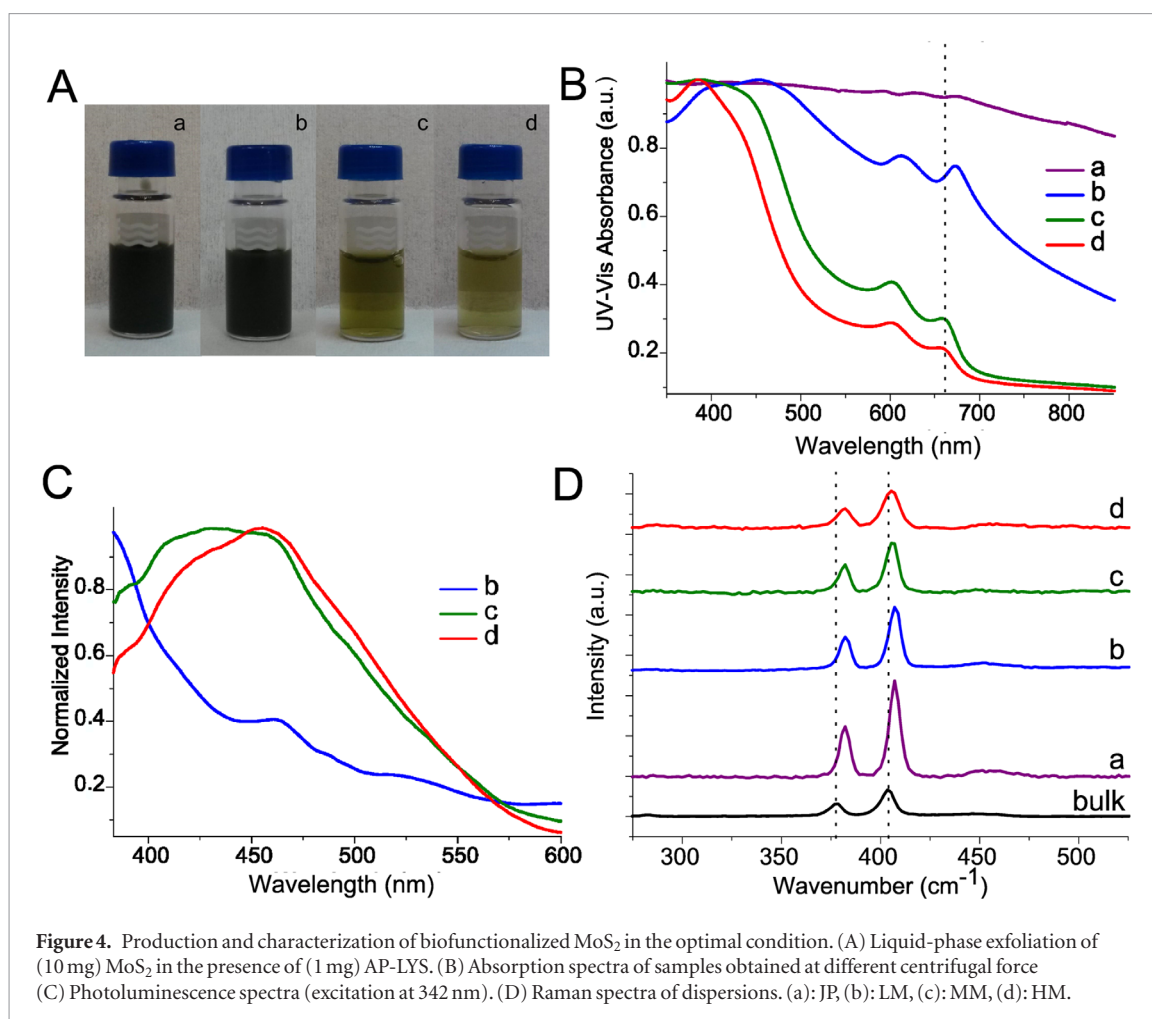
We also modelled fragment 1–18 alone (supp. figure S1 (stacks.iop.org/TDM/4/035007/mmedia)) in order to calculate a theoretical change in Gibbs free energy ΔG for the adsorption reaction:



The value we found, –5.3 kcal mol⁻¹ (corresponding to a binding constant $K = 1.7 \cdot 10^3$), suggests a relatively high affinity of fragment 1–18 for the MoS₂ surface. Taking into account that AP-LYS contains six additional amphipathic secondary structure elements which could contribute cooperatively to the binding, it can be concluded that the docking analysis supports the hypothesis that adsorption of AP-LYS to the MoS₂ surface is mediated by the binding of amphipathic regions of the denatured protein.

Optimization process

In order to verify the effect of AP-LYS in the exfoliation of MoS₂ a fixed amount of MoS₂ powder (10 mg) was mixed with increasing amounts of AP-LYS (from 0.5 mg to 5 mg) in 5 ml of 10 mM sodium acetate pH 5. After shaking overnight, the suspensions were sonicated for 7 h and subjected to centrifugation at increasing centrifugal forces (40 g, 2500 g and 4500 g). In the presence of the lowest amount of AP-LYS (0.5 mg, sample ‘a’ in figure 3(A)), the suspension appeared clear and colourless, whereas the rest of suspensions showed a yellow colour (samples from ‘b’ to ‘e’ in figure 3(A)). Hence, the suspensions were analysed by UV/Vis spectroscopy to determine the amount of MoS₂ in solution. In figure 3(B) the absorbance at 666 nm, which corresponds to the λ_{max} of a MoS₂ monolayer, is reported respectively as a function of the centrifugal force and amount of protein. In the presence of 0.5 mg of AP-LYS no MoS₂ was detectable in the solution. By increasing the amount of AP-LYS, from 0.5 mg to 1 mg (figures 3(B) and S2), the concentration of MoS₂ in solution significantly increased, and the maximum yield was obtained in the presence of 1 mg of AP-LYS. Increasing the amount of AP-LYS from 1 to 2 mg caused a decrease in the concentration of MoS₂ in solution but further increases (5 mg) caused no significant variation in the yield of soluble MoS₂ (figure 3(B)). The saturation at high concentrations of AP-LYS can be tentatively explained assuming that the effect of AP-LYS requires its adsorption onto the surface of MoS₂ crystals, once the surface becomes saturated any further increase in the concentration of the protein will not increase the exfoliation efficiency. Although it is not particularly straightforward to find a detailed explanation for the higher exfoliation yields obtained using 1 mg of AP-LYS, a similar behaviour has been previously observed exfoliating either MoS₂ in the presence of (deoxy)ribonucleotides [34] and BSA [39] or WS₂ in the presence of seaweed alginate [37]. This suggests that the existence of an optimal concentration of additive is a general feature of biomolecule-mediated exfoliation of 2D materials.



In order to optimize the production of MoS₂, different parameters were evaluated to achieve the best condition for the exfoliation: amount of starting material, MoS₂/protein ratios, AP-LYS concentration and ionic strength (figure S3(A)). All dispersions were sonicated (1 h) and centrifuged (40 g) in order to remove the non-exfoliated material. The amount of exfoliated material in suspension was determined spectrophotometrically (figures S3(C) and (E)). The highest yields of exfoliated material were obtained using a protein: MoS₂ ratio = 1:10 (w/w) and 0.2 mg ml⁻¹ of MoS₂ in the presence of 10 mM NaAc pH 5.

All the samples showed ζ -potential values in the range +24/+39 mV thus clearly indicating that the flakes of MoS₂ in suspension are covered by the cationic protein. The measured ζ -potential values are generally associated to particles with a moderate to good stability in suspension (figures S3(B) and (D)).

It is interesting to note that only in the case of the highest concentration of sodium acetate (30 mM) we obtained high standard deviations. These undesired variations among the replicates would suggest a reduced stability of the material at high ionic strength.

We performed the same set of experiment using a different starting material, such as graphite, to demonstrate that the AP-LYS is able to stabilize in a simple way different kinds of 2D materials (figure S4). Also in this case, different analyses were performed to evaluate the

optimal conditions needed to prepare a stable sample of graphene (figures S4–S7). The exfoliation yield of graphite is dependent on the amount of starting material and of stabilizer, as shown in the figure S4. So, since the starting material and also the lysozyme are low cost precursors, it is possible to increase the yield increasing their concentration. We obtained a high and significant concentration of graphene ($628 \pm 10 \mu\text{g ml}^{-1}$) decorated with positive charge (+32 mV) due to the AP-LYS coating (figure S5). The exfoliation of graphite was confirmed by SEM images and Raman spectroscopy (figures S6 and S7).

Production and stabilization of MoS₂ by AP-LYS

The exfoliated material obtained using the optimal experimental conditions as described in the previous section was thoroughly characterized. When the exfoliation, attempted in the absence of protein, produced a dark dispersion, that resulted clear without any detectable MoS₂, after gentle centrifugation (see figure S8).

Figure 4(A) shows the dispersions obtained after exfoliation (called JP, just prepared) and after centrifugation at different centrifugal force 40 g (called LM, low MoS₂), 2500 g (called MM, medium MoS₂) and 4500 g (called HM, high MoS₂). Thanks to the centrifugation process we separate the MoS₂ classes.

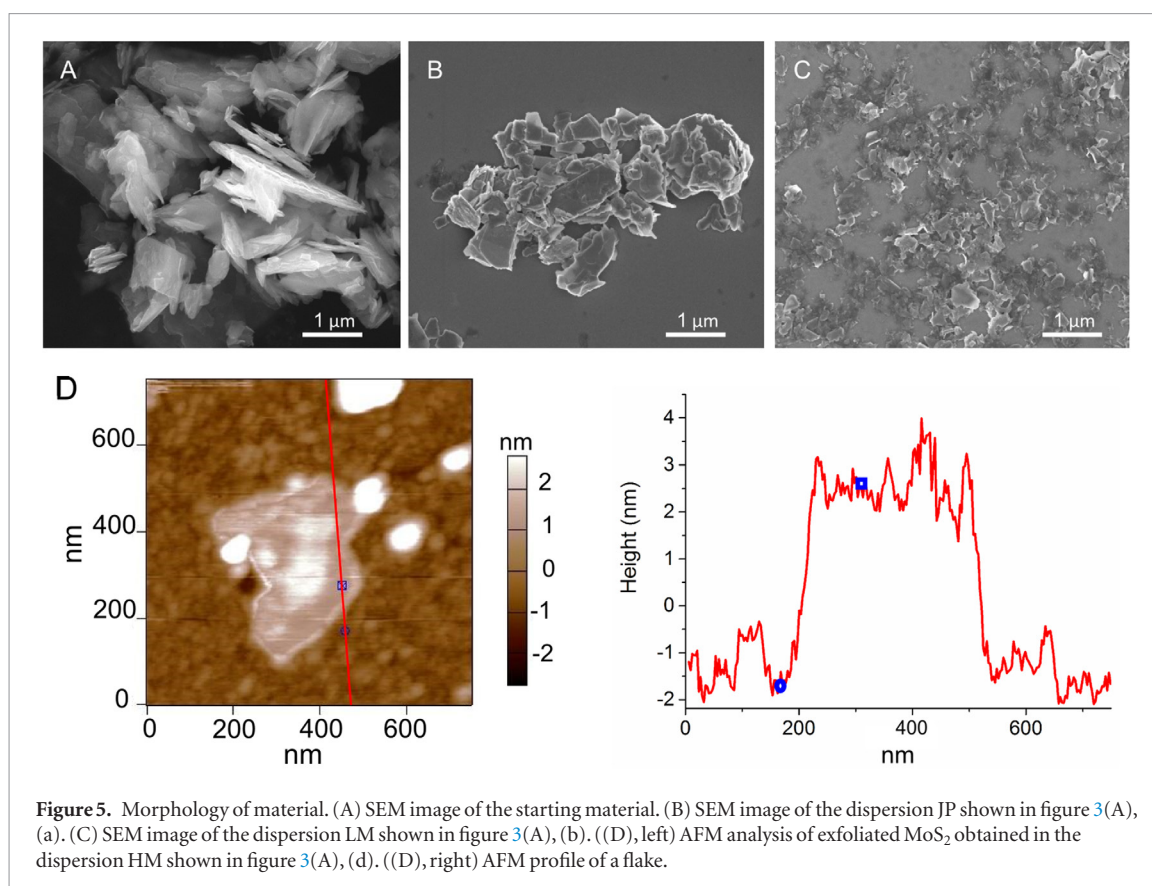


Figure 5. Morphology of material. (A) SEM image of the starting material. (B) SEM image of the dispersion JP shown in figure 3(A), (a). (C) SEM image of the dispersion LM shown in figure 3(A), (b). ((D), left) AFM analysis of exfoliated MoS₂ obtained in the dispersion HM shown in figure 3(A), (d). ((D), right) AFM profile of a flake.

Table 1. Stability, electrophoretic mobility and absorbance of MoS₂ dispersions.

Centrifugal force (g)	ζ -Potential (mV)	Electrophoretic mobility ($\mu\text{m s}^{-1} \text{cm V}^{-1}$)	Absorbance at 666 nm (O.D.)
40	25.3 ± 1.8	1.984 ± 0.137	18.05 ± 1.23
2500	26.8 ± 1.1	2.104 ± 0.088	0.399 ± 0.025
4500	28.7 ± 2.9	2.249 ± 0.323	0.196 ± 0.001

The colour of dispersion changed from dark greenish to a yellowish suspension, indicating that the concentration decreased increasing the centrifugal force and in the same time the sample reached a smaller size (figure 4(A)).

SEM imaging was used to characterize the morphology of the starting material and that of the MoS₂ delaminated in presence of AP-LYS. The starting material was characterized by the presence of crystallites of 1–2 μm lateral size (figure 5(A)). Exfoliated material showed, with the increase of centrifugal force, a gradual decrease in the particle size (figures 5(B) and (C)).

The UV–Vis absorption spectra showed a progressive blue-shift of the peak at 687, typical of bulk MoS₂ from the JP to the HM dispersion due to a decrease in the number of layers (figure 4(B)) [38, 62]. The MM and HM dispersions showed a narrowed main peak centered at 387 nm and a minor peak at 666 nm typical of single layer MoS₂ nanosheet [30, 63]. The average number of layers present in each population, calculated as described previously [63, 64], progressively decreased from 9.6 in the LM sample to 1.3 in the HM sample (table S2). As expected, increasing the cen-

trifugal force, the yield in the exfoliation dramatically decreased from 18.05 to 0.196 O.D (table 1), obtaining MoS₂ of 180 $\mu\text{g ml}^{-1}$ (HM sample).

All dispersions showed a positive ζ -potential due to the adsorption of the cationic protein to the surface. Very interestingly, the highest value was measured for the HM sample. To further confirm the cationic nature of the exfoliate material, we also characterized the electrokinetic behaviour of LM, MM and HM. All the samples migrated toward the negative electrode with electrophoretic mobility (U_e) of $1.984 \pm 0.137 \mu\text{m s}^{-1} \text{cm V}^{-1}$, $2.104 \pm 0.088 \mu\text{m s}^{-1} \text{cm V}^{-1}$ and $2.249 \pm 0.323 \mu\text{m s}^{-1} \text{cm V}^{-1}$ in the case of for LM, MM and HM samples, respectively. The progressive increase of the electrophoretic mobility is in good agreement with the ζ -potential values (table 1, figure S9). Since the protein is positive and the MoS₂ surface is nonpolar this charge is due to their assembling through the adsorption of charged AP-LYS molecules onto the MoS₂ surface. Furthermore, the LM, MM and HM samples showed a progressively increasing photoluminescence emission at 455 nm (figure 4(C)).

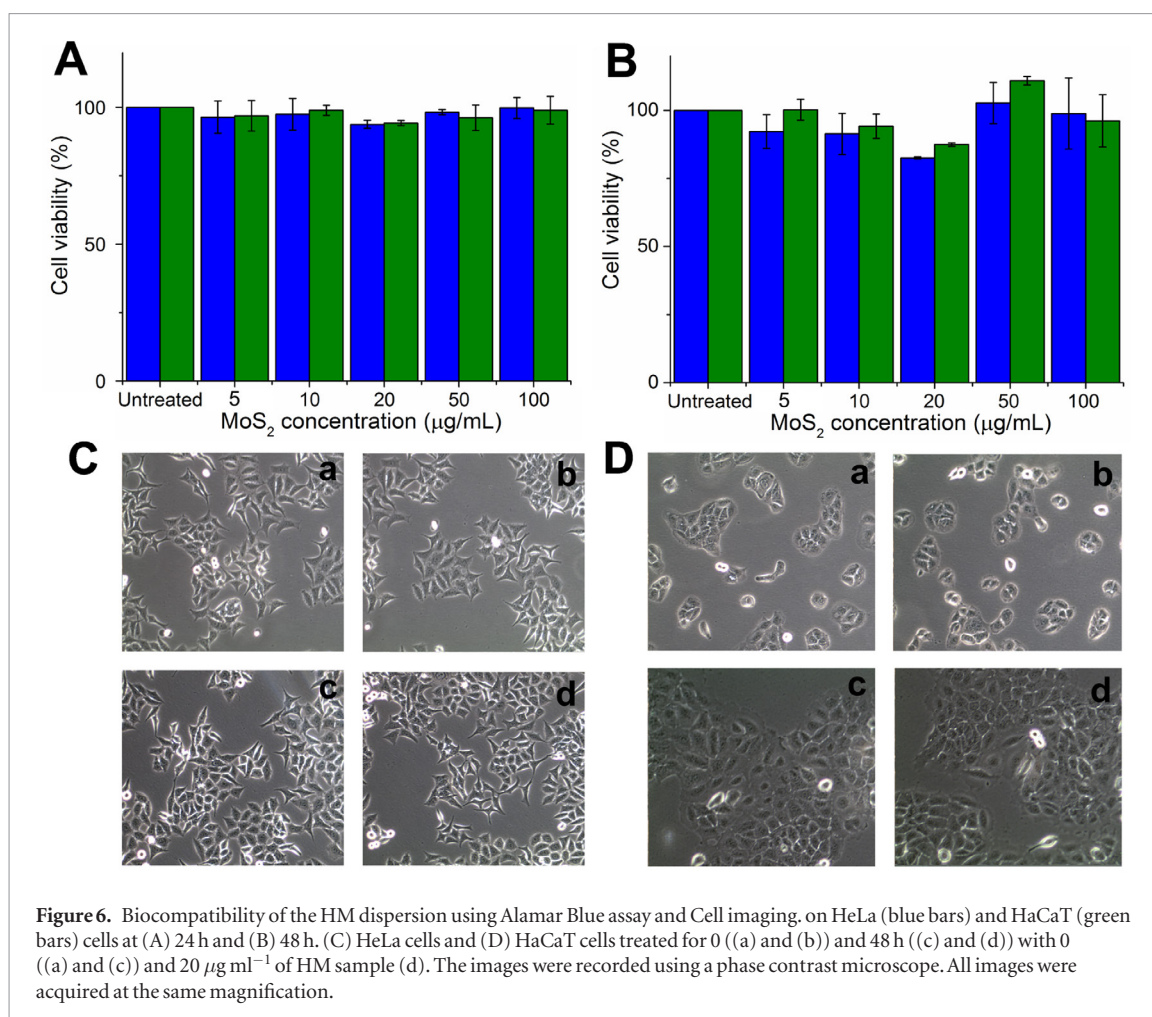


Figure 6. Biocompatibility of the HM dispersion using Alamar Blue assay and Cell imaging, on HeLa (blue bars) and HaCaT (green bars) cells at (A) 24 h and (B) 48 h. (C) HeLa cells and (D) HaCaT cells treated for 0 ((a) and (b)) and 48 h ((c) and (d)) with 0 ((a) and (c)) and 20 $\mu\text{g ml}^{-1}$ of HM sample (d). The images were recorded using a phase contrast microscope. All images were acquired at the same magnification.

We also characterized the Raman spectrum of the studied dispersions (figure 4(D)). From the bulk material to the HM sample, we measured a red shift of the two bands E_{2g}^1 and A_{1g} , respectively associated with the in-plane vibration and out-of-plane vibration, from 379 and 404 cm^{-1} to 382 and 405 cm^{-1} [39, 65]. The red shift of E_{2g}^1 band is indicator of a reduction in the number of layers [2, 66], however, the Raman spectrum of mechanically exfoliated MoS₂ monolayers usually show a blue shift of the A_{1g} band instead of the red shift we observed. A possible explanation of this difference is that, differently from the E_{2g}^1 band, the A_{1g} band is strongly influenced by surface adsorption and electron doping events and can even undergo a red shift depending on the environment conditions [2, 39, 67]. Therefore, the observed red shift could be caused by the adsorption of AP-LYS at the surface of the layers.

Additionally, atomic force microscopy confirmed the production of MoS₂ flakes with a thickness of 5 nm (see figures 5(D) and S10). On the basis of the lysozyme height obtained through the AFM analysis (figure S11) we could assess that, in agreement with the results obtained from the UV-Vis analysis, the exfoliation process gave rise to monolayer MoS₂ nanosheets with lysozyme adsorbed onto both surfaces of the flakes. Moreover, the statistical analysis of the lateral size showed that most of the flakes had lateral sizes between 250 and 550 nm (figure S12).

Biocompatibility

In order to analyse the biocompatibility of MoS₂, the stability of the HM sample in physiological conditions was evaluated by monitoring its UV-Vis after 48 h incubation time (figure S13). No difference was observed in the peak at 666 nm of the sample incubated in PBS buffer, 10% FBS in 10 mM NaAc pH 5.0 or 10% FBS in PBS buffer (figure S13), thus suggesting that neither PBS nor FBS induce a significant alteration in the stability of the AP-LYS coated flakes.

Therefore, the biocompatibility of the HM sample was analysed using two model human cell lines, human cancer epithelial cells (HeLa cells) and human normal keratinocytes (HaCaT cells). The cells were treated with increasing amounts of the HM sample (from 5 to 100 $\mu\text{g ml}^{-1}$) for 24 and 48 h. As shown in figures 6(A) and (B), cell viability was not affected at any of the concentration tested, up to 48 h incubation ($p > 0.05$). Moreover, the cells did not show any change in their morphology (figures 6(C) and (D)), thus indicating that this new material was completely biocompatible.

In order to highlight the better efficiency of AP-LYS to biofunctionalize MoS₂ in aqueous solution, we compared our results with those obtained by Guan *et al* (2015) [39] using BSA (table S3). Even if both proteins are able to exfoliate MoS₂, the procedures show several differences in terms of exfoliation time, yield and production rate. We produced 430 $\mu\text{g ml}^{-1}$ of MoS₂ after

a sonication for 7 h, resulting in a yield of 21.5%, this value is lower than that obtained by Guan *et al* (1360 $\mu\text{g ml}^{-1}$, 27.2%). In contrast, when we compare the exfoliation rate, we reached a production rate that is six times higher in order of magnitude (61.4 $\mu\text{g ml}^{-1} \text{h}^{-1}$). Furthermore, the concentration of AP-LYS is five times lower than that used by Guan *et al*. Moreover, using AP-LYS, the ratio between starting material and protein (MoS_2 : protein) is two times lower than the other one. This behaviour is due to the nature of denatured protein that has all residues exposed to the surface, thus it can interact with MoS_2 surface in excellent way. Finally, we found that the exfoliated material we obtained had no effect on cell viability (100% cell survival) up to 48 h incubation and to 100 $\mu\text{g ml}^{-1}$, with respect to Guan, who found a 30% of cell death after 24 h with 10 $\mu\text{g ml}^{-1}$. These differences are due to the unfolded nature of AP-LYS; while conventional 3D proteins, like BSA, have the hydrophobic residues in the core, exposing the hydrophilic residues [21], on the contrary, denatured lysozyme totally exposes the hydrophobic groups, increasing the surface area and the flexibility thus optimizing the interaction with the MoS_2 surface. Moreover, thanks to this modification, AP-LYS enhances in terms of positive charge surrounding the material surface, which is useful for the binding of negatively charged agents, such as DNA, RNA, antibody, or other materials, such as gold nanoparticle. These advantages make denatured lysozyme a very promising bio-tool for the functionalization of MoS_2 and other 2D materials.

Conclusions

We demonstrated a simple approach to exfoliate MoS_2 in aqueous media through the use of biofunctionalization agent (AP-LYS), making it biocompatible and useful for bio-applications. We proved that this method can be applied to different starting materials, such as graphite and molybdenum disulphide, using AP-LYS. Given the exposure of hydrophobic groups, AP-LYS is an advantageous biomaterial to stabilize and functionalize MoS_2 , obtaining high quality MoS_2 flakes. Furthermore, by centrifuging the sample at different centrifugal force it is possible to select MoS_2 classes with different layers. Thanks to AP-LYS coating, we produced highly stable and biocompatible MoS_2 dispersions with a positive charge providing an optimal surface for a wide range of applications with interest for applications in bionanotechnology and biomedicine. Overall, this approach allows for the production of different bio-hybrid materials, opening the way for the development and production of other remarkable biocompatible 2D materials.

Acknowledgments

ICN2 acknowledges support from the Severo Ochoa Program (MINECO, Grant SEV-2013-0295).

The Nanobiosensors and Bioelectronics Group acknowledges the support from the Generalitat de Catalunya (Grant 2014 SGR 260).

References

- [1] Gupta A, Sakhivel T and Seal S 2015 *Prog. Mater. Sci.* **73** 44
- [2] Gan X, Zhao H and Quan X 2017 Two-dimensional MoS_2 : a promising building block for biosensors *Biosens. Bioelectron.* **89** 59–71
- [3] Ataca C, Sahin H and Ciraci S 2012 *J. Phys. Chem. C* **116** 8983
- [4] Huang Y H, Peng C C, Chen R S, Huang Y S and Ho C H 2014 *Appl. Phys. Lett.* **105** 93106
- [5] Huang J, Dong Z, Li Y, Li J, Tang W, Yang H, Wang J, Bao Y, Jin J and Li R 2013 *Mater. Res. Bull.* **48** 4544
- [6] Li X, Shan J, Zhang W, Su S, Yuwen L and Wang L 2016 *Small* **13** 1602660
- [7] Ganatra R and Zhang Q 2014 *ACS Nano* **8** 4074
- [8] Heine T 2015 *Acc. Chem. Res.* **48** 65
- [9] Roxlo C B, Chianelli R R, Deckman H W, Ruppert A F and Wong P P 1987 *J. Vac. Sci. Technol. A* **5** 555
- [10] Mak K F, Lee C, Hone J, Shan J and Heinz T F 2010 *Phys. Rev. Lett.* **105** 136805
- [11] Cheng Y, Wang J Z, Wei X X, Guo D, Wu B, Yu L W, Wang X R and Shi Y 2015 *Chin. Phys. Lett.* **32** 4
- [12] Chhowalla M 2012 *Nano Lett.* **12** 526
- [13] Splendiani A, Sun L, Zhang Y, Li T, Kim J, Chim C Y, Galli G and Wang F 2010 *Nano Lett.* **10** 1271
- [14] Zhang W, Huang J K, Chen C H, Chang Y H, Cheng Y J and Li L J 2013 *Adv. Mater.* **25** 3456
- [15] Tsai M L, Su S H, Chang J K, Tsai D S, Chen C H, Wu C I, Li L J, Chen L J and He J H 2014 *ACS Nano* **8** 8317
- [16] Liu B, Chen L, Liu G, Abbas A N, Fathi M and Zhou C 2014 *ACS Nano* **8** 5304
- [17] Wang Y *et al* 2013 *ACS Nano* **7** 10083
- [18] He Z and Que W 2016 *Appl. Mater. Today* **3** 23
- [19] Geim A K and Grigorieva I V 2013 *Nature* **499** 419
- [20] Naylor C H, Kybert N J, Schneier C, Xi J, Romero G, Saven J G, Liu R and Johnson A T C 2016 *ACS Nano* **10** 6173
- [21] Paredes J I and Villar-Rodil S 2016 *Nanoscale* **8** 15389
- [22] Lopez-Sanchez O, Lembke D, Kayci M, Radenovic A and Kis A 2013 *Nat. Nanotechnol.* **8** 497
- [23] Gao N, Zhou W, Jiang X, Hong G, Fu T-M and Lieber C M 2015 *Nano Lett.* **15** 2143
- [24] Zhang Y, Zhang L and Zhou C 2013 *Acc. Chem. Res.* **46** 2329
- [25] Han G H *et al* 2015 *Nat. Commun.* **6** 128
- [26] Niu L, Coleman J N, Zhang H, Shin H, Chhowalla M and Zheng Z 2016 *Small* **12** 272
- [27] Hernandez Y, Lotya M, Rickard D, Bergin S D and Coleman J N 2010 *Langmuir* **26** 3208
- [28] Jiang F *et al* 2016 *J. Mater. Chem. A* **4** 5265
- [29] Dileep K, Sahu R, Sarkar S, Peter S C and Datta R 2016 *J. Appl. Phys.* **119** 114309
- [30] Varrla E, Backes C, Paton K R, Harvey A, Gholamvand Z, McCauley J and Coleman J N 2015 *Chem. Mater.* **27** 1129
- [31] Smith R J *et al* 2011 *Adv. Mater.* **23** 3944
- [32] Ciesielski A *et al* 2016 *ACS Nano* **10** 10768
- [33] Lim C T and Kenry K 2016 *ChemNanoMat* **3** 5
- [34] Ayán-Varela M *et al* 2017 *ACS Appl. Mater. Interfaces* **9** 2835–45
- [35] Li Y, Zhu H, Shen F, Wan J, Lacey S, Fang Z, Dai H and Hu L 2015 *Nano Energy* **13** 346
- [36] Feng X, Wang X, Xing W, Zhou K, Song L and Hu Y 2014 *Compos. Sci. Technol.* **93** 76
- [37] Zong L, Li M and Li C 2017 *Adv. Mater.* **29** 1604691
- [38] Bang G S, Cho S, Son N, Shim G W, Cho B-K and Choi S-Y 2016 *ACS Appl. Mater. Interfaces* **8** 1943
- [39] Guan G *et al* 2015 *J. Am. Chem. Soc.* **137** 6152
- [40] Ge Y, Wang J, Shi Z and Yin J 2012 *J. Mater. Chem.* **22** 17619
- [41] Forsberg V, Zhang R, Bäckström J, Dahlström C, Andres B, Norgren M, Andersson M, Hummelgård M and Olin H 2016 *PLoS One* **11** e0154522

- [42] Siepi M, Politi J, Dardano P, Amoresano A, De Stefano L, Monti D M and Notomista E 2017 *Nanotechnology* (<https://doi.org/10.1088/1361-6528/aa744e>)
- [43] Donadio G, Sarcinelli C, Pizzo E, Notomista E, Pezzella A, Di Cristo C, De Lise F, Di Donato A and Izzo V 2015 *PLoS One* **10** e0124427
- [44] De Rosa M, Zanfardino A, Notomista E, Wichelhaus T A, Saturnino C, Varcamonti M and Soriente A 2013 *Eur. J. Med. Chem.* **69** 779
- [45] Notomista E, Cafaro V, Bozza G and Di Donato A 2009 *Appl. Environ. Microbiol.* **75** 823
- [46] Notomista E, Scognamiglio R, Troncone L, Donadio G, Pezzella A, Di Donato A and Izzo V 2011 *Appl. Environ. Microbiol.* **77** 5428
- [47] Zanfardino A, Restaino O F, Notomista E, Cimini D, Schiraldi C, De Rosa M, De Felice M and Varcamonti M 2010 *Microb. Cell Fact.* **9** 34
- [48] Zhorov B S and Bregestovski P D 2000 *Biophys. J.* **78** 1786
- [49] Weiner S J, Kollman P A, Case D A, Singh U C, Ghio C, Alagona G, Profeta S and Weiner I P 1984 *J. Am. Chem. Soc.* **106** 765
- [50] Lazaridis T and Karplus M 1999 *Proteins Struct. Funct. Genet.* **35** 133
- [51] Lazaridis T and Karplus M 1999 *J. Mol. Biol.* **288** 477
- [52] Li L, Morrill M R, Shou H, Barton D G, Ferrari D, Davis R J, Agrawal P K, Jones C W and Sholl D S 2013 *J. Phys. Chem. C* **117** 2769
- [53] Guex N and Peitsch M C 1997 *Electrophoresis* **18** 2714
- [54] Lotya M et al 2009 *J. Am. Chem. Soc.* **131** 3611
- [55] Kelly S M, Jess T J and Price N C 2005 *Biochim. Biophys. Acta* **1751** 119
- [56] Reiersen H and Rees A R 2000 *Protein Eng.* **13** 739
- [57] Carlier L, Joanne P, Khemtémourian L, Lacombe C, Nicolas P, El Amri C and Lequin O 2015 *Biophys. Chem.* **196** 40
- [58] Lequin O, Ladram A, Chabbert L, Bruston F, Convert O, Vanhoye D, Chassaing G, Nicolas P and Amiche M 2006 *Biochemistry* **45** 468
- [59] Wang L, Wang D and Li F 2014 *J. Pept. Sci.* **20** 165
- [60] Di Natale G, Pappalardo G, Milardi D, Sciacca M F M, Attanasio F, La Mendola D and Rizzarelli E 2010 *J. Phys. Chem. B* **114** 13830
- [61] Yang J J, Buck M, Pitkeathly M, Kotik M, Haynie D T, Dobson C M and Radford S E 1995 *J. Mol. Biol.* **252** 483
- [62] Sreedhara M B, Matte H S S R, Govindaraj A and Rao C N R 2013 *Chem. Asian J.* **8** 2430
- [63] Backes C et al 2014 *Nat. Commun.* **5** 4576
- [64] Kaur J, Gravagnuolo A M, Maddalena P, Altucci C, Giardina P and Gesuele F 2017 *RSC Adv.* **7** 22400
- [65] Zeng Z, Yin Z, Huang X, Li H, He Q, Lu G, Boey F and Zhang H 2011 *Angew. Chem., Int. Ed. Engl.* **50** 11093
- [66] Li H, Zhang Q, Yap C C R, Tay B K, Edwin T H T, Olivier A and Baillargeat D 2012 *Adv. Funct. Mater.* **22** 1385
- [67] Chakraborty B, Bera A, Muthu D V S, Bhowmick S, Waghmare U V and Sood A K 2012 *Phys. Rev. B* **85** 161403